Supporting Information

Ultrahigh-Capacity and Dendrite-free Lithium Metal Anodes enabled by Lithiophilic Bimetallic Oxides

Yang Yang, [a#] Jiaqi Cao,[a#] Wangyang Li,[a#] Qiaoli Zhang,[a] Yonghui Xie,[a] Yunda Lai,[a] Shuying Cheng,[a, b, c] Baihua Qu,[d] Dong-Liang Peng,[e] Xinghui Wang[a, b, c, f*]

[a] *College of Physics and Information Engineering, Institute of Micro-Nano Devices and Solar Cells, Fuzhou University, Fuzhou, 350108, China.*

[b] *Fujian Science & Technology Innovation Laboratory for Optoelectronic Information of China, Fuzhou, Fujian 350108, China.*

[c] *Jiangsu Collaborative Innovation Center of Photovoltaic Science and Engineering, Changzhou, 213000, China.*

[d] *College of Materials Science and Engineering, Chongqing University, Chongqing，400044, PR China.*

[e] *College of Materials, Xiamen University, Xiamen, 361005, PR China.*

[f] *Fujian Key Laboratory of Electrochemical Energy Storage Materials, Fuzhou University, Fuzhou, Fujian 350002, China.*

[*] **Corresponding author: seaphy23@fzu.edu.cn.**

# These authors contributed equally to this work.

1. Experimental Section

1.1. Material Synthesis

Synthesis of ZMO@CC: The commercial carbon cloths (4 × 4 cm) were treated with concentrated HNO_3 before use. The CC was immersed in a Teflon-lined stainless autoclave with a precursor solution (40 ml) that contained $ZnSO_4 \cdot 7H_2O$ (0.25 mmol) and $KMnO_4$ (0.5 mmol). After hydrothermally treated at 160 ℃ for 24 h, the CC sample was cleaned with DI water and then annealed in air at 300 ℃ for 2 h to obtain the ZMO@CC.

Synthesis of ZCO@CC: The hydrothermally treated process was similar to the previous work[43].The CC was immersed in a Teflon-lined stainless autoclave with a precursor solution (50 ml) that contained $Zn(NO_3)_2 \cdot 6H_2O$ (1 mmol), $Co(NO_3)_2 \cdot 6H_2O$ (2 mmol), NH_4F (2 mmol), and $CO(NH_2)_2$ (5 mmol). After hydrothermally treated at 120 ℃ for 10 h, the CC sample was cleaned with DI water and then annealed in air at 300 ℃ for 2 h to obtain the ZCO@CC.

Synthesis of NCO@CC: The hydrothermally treated process was similar to the previous work[44].The CC was immersed in a Teflon-lined stainless autoclave with a precursor solution (50 ml) that contained $Ni(NO_3)_2 \cdot 6H_2O$ (1 mmol), and $Co(NO_3)_2 \cdot 6H_2O$ (2 mmol), $CO(NH_2)_2$ (8 mmol). After hydrothermally treated at 120 ℃ for 10 h, the CC sample was cleaned with DI water and then annealed in air at 350 ℃ for 2 h to obtain the NCO@CC.

Synthesis of MnO_2@CC: The CC was immersed in a Teflon-lined stainless autoclave with a precursor solution (50 ml) that contained $KMnO_4$ (0.5 mmol). After hydrothermally treated at 160 ℃ for 24 h, the CC sample was cleaned with DI water and then annealed in air at 300 ℃ for 2 h to obtain the MnO_2@CC.

Synthesis of ZnO@CC[45]: To obtain the ZnO@CC, a simple annealing treatment was employed. $Zn(NO_3)_2 \cdot 6H_2O$ was dissolved in DI water with a concentration of 100 mg

46 mL^{-1}. After being immersed in $Zn(NO_3)_2$ solution for 10 min, the CC was taken out and
47 calcined in a tube furnace (BEQ, BTF 1200C) at 500 °C for 10 min in argon, and then
48 the ZnO@CC was obtained.

49 ***Fabrication of Composite Li Anodes (Li-ZMO@CC, Li-ZCO@CC, Li-NCO@CC, Li-***
50 ***MnO_2@CC, and Li-ZnO@CC)***

51 Firstly, the as-fabricated samples were cut into disks with a diameter of 12 mm.
52 The molten infusion process was carried out in an argon-filled glove box. The Li foils
53 were molten in a stainless-steel container at 300 °C. Subsequently, the Li-ZMO@CC,
54 Li-ZCO@CC, Li-NCO@CC, Li-MnO_2@CC, and Li-ZnO@CC were obtained by
55 directly contacting molten Li with ZMO@CC, ZCO@CC, NCO@CC, MnO_2@CC, and
56 ZnO@CC, respectively.

57 **1.2. Electrochemical Measurements**

58 Symmetric cells were employed to investigate the electrochemical cycling
59 performance and assembled in an argon-filled glove box. CR2032-type coin cells were
60 used for assembling the symmetric cell with two identical electrodes (Li foil or the as-
61 fabricated composite Li Anodes). The electrolyte was ether-based electrolyte, including
62 a mixture of 1M lithium salt (LiTFSI) dissolved in in 1,3-dioxolane (DOL) and 1,2-
63 dimethoxyethane (DME) (v/v=1:1) with 1% $LiNO_3$, while the separator was Celgard
64 2400. The amount of electrolyte employed for each cell was 40 μL. The electrochemical
65 cycling performance were conducted on the Neware multichannel battery tester (CT-
66 4008). Electrochemical impedance spectroscopy (EIS) measurements were tested on a
67 Bio-Logic VSP multichannel electrochemical workstation with 0.01 Hz to 100 kHz.

68 For full cell, the $LiFePO_4$ (LFP) cathodes (active mass loading: 3.5 mg cm^{-2}) were
69 prepared by blade-casting the mixed slurry containing LFP powder, carbon black, and
70 polyvinylidene fluoride (mass ratio of 8:1:1) onto the aluminum foil, following a
71 vacuum drying process at 120 °C for overnight. The pouch cell with size of 4 × 2 cm^2

was assembled in the glove box by pairing composite Li anode and LFP cathode (active mass loading: 16 mg).

1.3. Materials characterization

A scanning electron microscope (SEM, Helios G4 CX, FEI) equipped with an energy dispersive X-ray spectrometer (EDX) was employed to observe the morphology and chemical element distribution of the samples. The XRD patterns were measured by Rigaku SmartLab (Cu Kα radiation, 40 kV, 30 mA). To avoid air pollution of Li, the electrode after Li infusion was encapsulated in CR2032 case (Shenzhen Kejing) with one side Kapton window before the XRD analysis. XPS analysis was explored by an X-ray photoelectron spectrometer (Thermo Scientific K-Alpha, Al Kα radiation). TEM and SAED were performed on a field emission transmission electron microscope (JEOL JEM-2100F).

1.4. Operando Optical Testing

The optical microscopy videos were taken with a 6XB-PC Shanghai Guangxue microscope at 10X with a plan objective. A sealed electrochemical pool (STC-Q Shenzhen Kejing) using ether-based electrolyte was used for visualization in-situ morphology studies. The electrochemical measurements during the in-situ processes were carried out on a Bio-Logic VSP multichannel electrochemical workstation.

1.5. Theoretical calculations

Theoretical calculations were performed using the Vienna Ab Initio Simulation Package (VASP) with the ionization potentials, including the effect of core electrons, being described by the projector augmented wave (PAW) method [46, 47]. In this work, the Perdew−Burke−Ernzerhof (PBE) GGA exchange−correlation functionals were used to relax the structures of compounds of interest, which h can be obtained from material projects, such as $ZnMn_2O_4$(mp-18751), $ZnCo_2O_4$(mp-753489), $NiCo_2O_4$(mp-

1096547), MnO_2(mp-510408), ZnO(mp-2133), Li(mp-51), Mn(mp-35), LiZn(mp-1934), Li_2O(mp-1960), Ni(mp-23), Co(mp-102). A plane-wave energy cutoff of 500 eV is used in all calculations. For the geometric relaxation of the structures, a summation over the Brillouin Zone (BZ) was performed with the Monkhorst–Pack k-point with spacing smaller than 0.04 $Å^{-1}$ to guarantee precision. All structures are geometrically relaxed until the total force on each ion was reduced below 0.01 eV $Å^{-1}$. The bulk Gibbs free energy can be assessed with the consideration of the dictating phonon entropy for each phase[48]. Therefore, the Gibbs free energy change (ΔG) between products and reactants can be quantified as follows:

$$\Delta G = (G_{products} - G_{reactants})/n,$$

where n is the number of atoms in products or reactants.

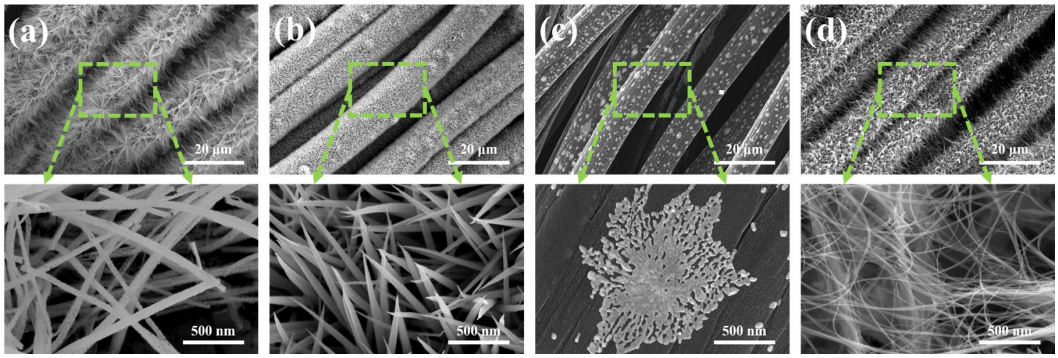

Fig. S1. SEM images of different bimetallic and monometallic oxides. (a) ZCO@CC, (b) NCO@CC, (c) ZnO@CC, and (d) MnO_2@CC.

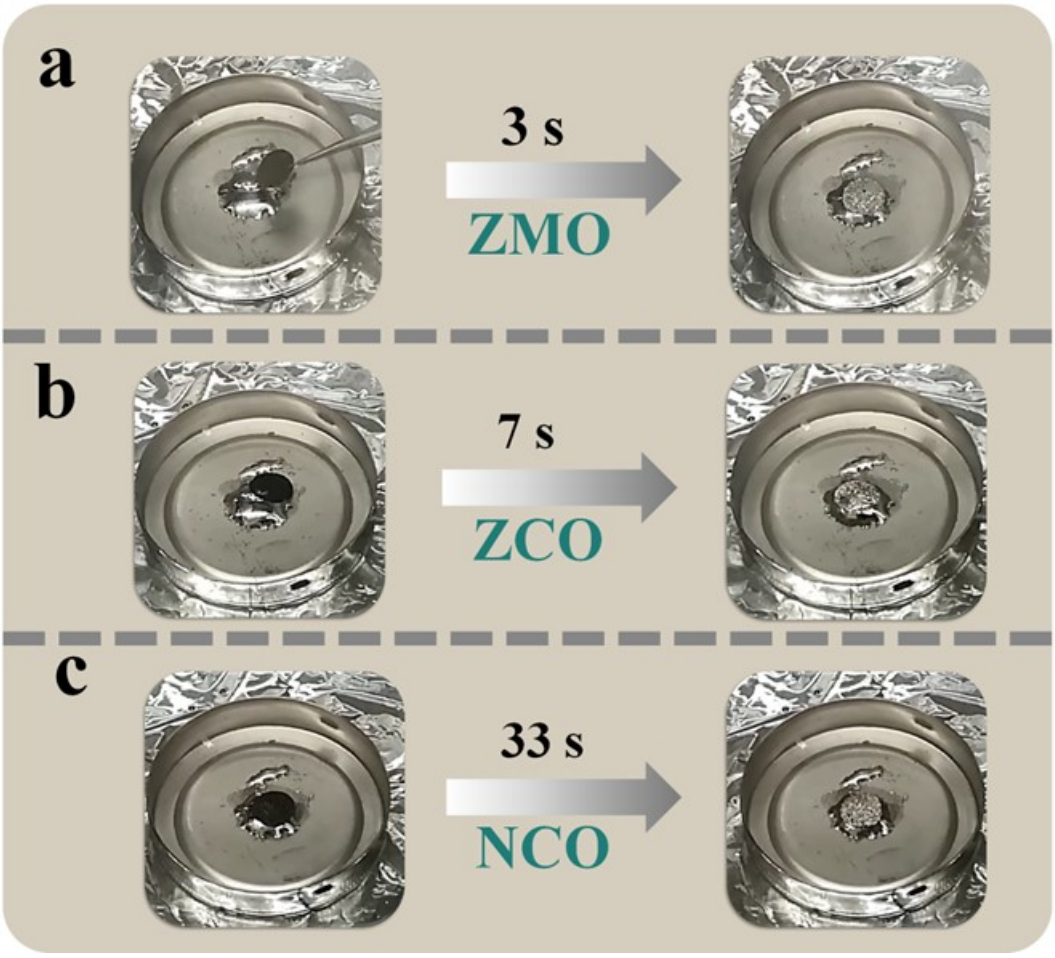

Fig. S2. Digital images of molten Li infusing processes. Time-lapse images for Li-metal infusion of (a) ZMO@CC, (b) ZCO@CC, (c) NCO@CC.

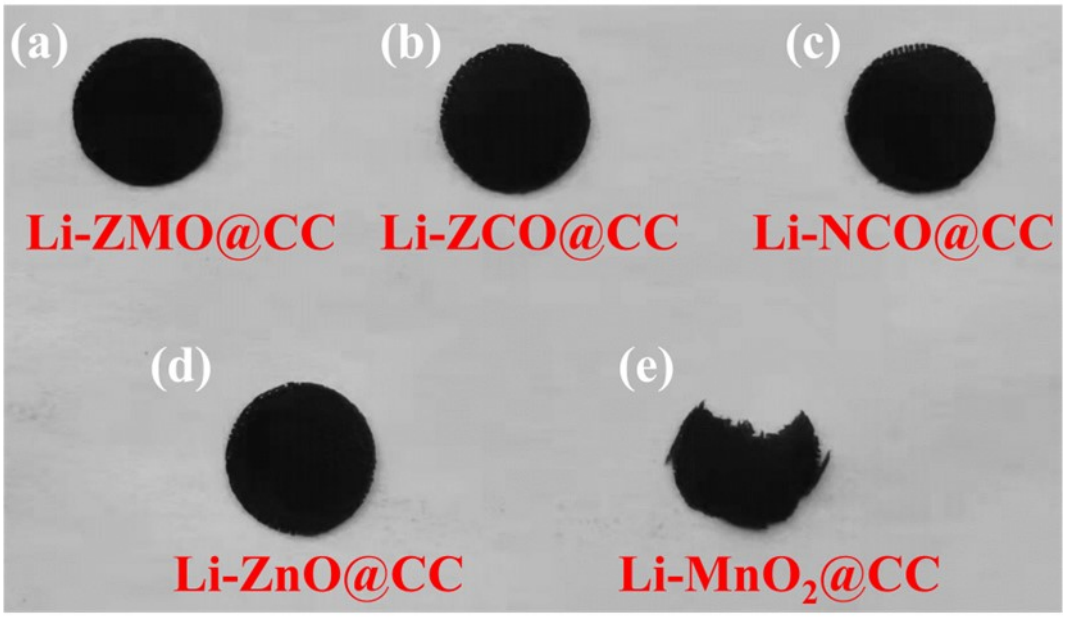

Fig. S3. Digital images of the composite Li anodes after removing Li metal. The digital camera images of (a) Li-ZMO@CC, (b) Li-ZCO@CC, (c) Li-NCO@CC, (d) Li-ZnO@CC, and (e) Li-MnO_2@CC after removing Li via absolute ethyl alcohol.

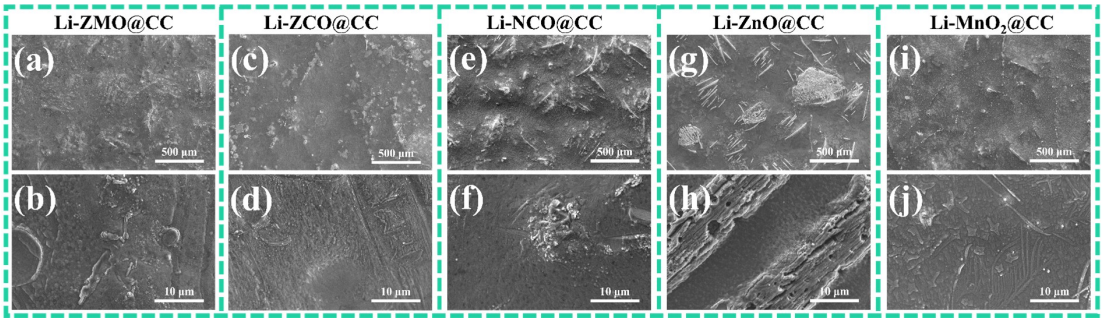

Fig. S4. Morphology characterizations of composite Li anodes. The SEM images of (a-b) Li-ZMO@CC, (c-d) Li-ZCO@CC, (e-f) Li-NCO@CC, (g-h) Li-ZnO@CC, and (i-j) Li-MnO_2@CC.

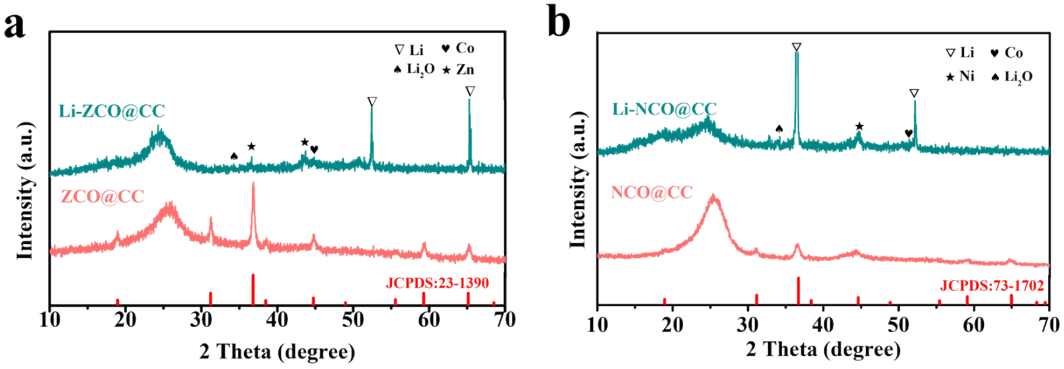

Fig. S5. Characterization of the electrodes before and after molten Li. The XRD patterns of (a) ZCO@CC and Li-ZCO@CC, (b) NCO@CC and Li-NCO@CC, respectively.

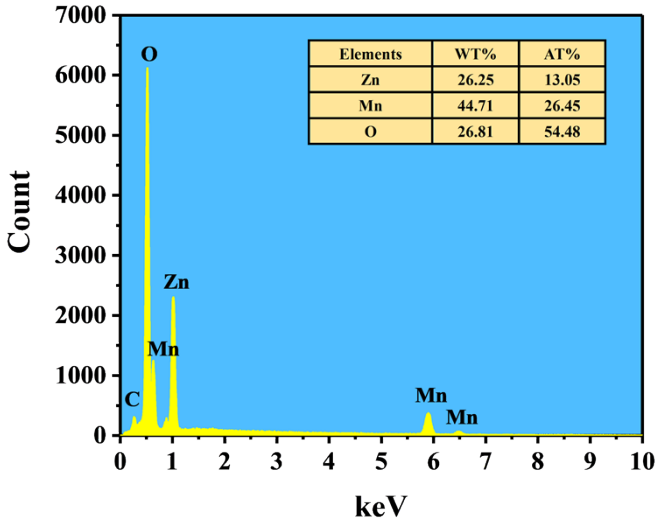

Elements	WT%	AT%
Zn	26.25	13.05
Mn	44.71	26.45
O	26.81	54.48

Fig. S6. EDX spectrum of ZMO@CC.

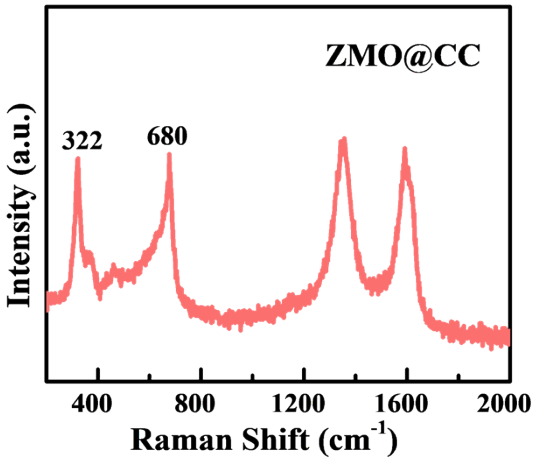

Fig. S7. Raman spectra of ZMO@CC.

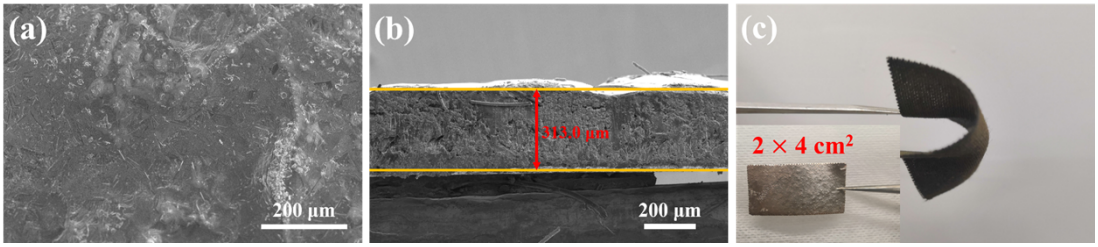

Fig. S8. Morphology characterizations of Li-ZMO@CC**.** The (a) surface and (b) cross-sectional SEM images of Li-ZMO@CC. (c) Digital images of ZMO@CC and Li-ZMO@CC (the inset).

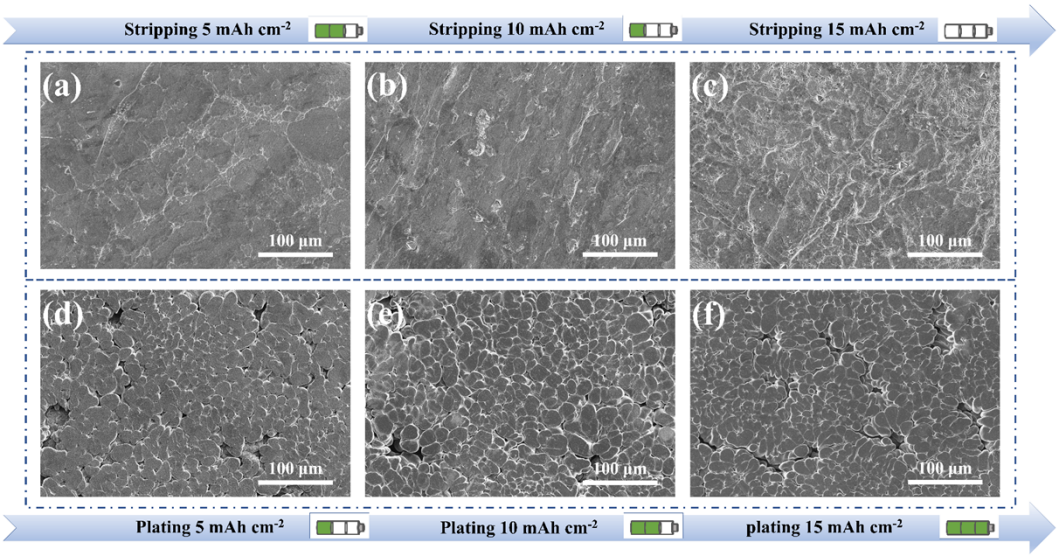

Fig. S9. Morphology of Li foil during stripping/plating. The stripping capacity of (a) 5 mAh cm^{-2}, (b) 10 mAh cm^{-2}, (c) 15 mAh cm^{-2}, and then replating capacity of (d) 5 mAh cm^{-2}, (e) 10 mAh cm^{-2}, and (f) 15 mAh cm^{-2} at a current density of 1 mA cm^{-2}.

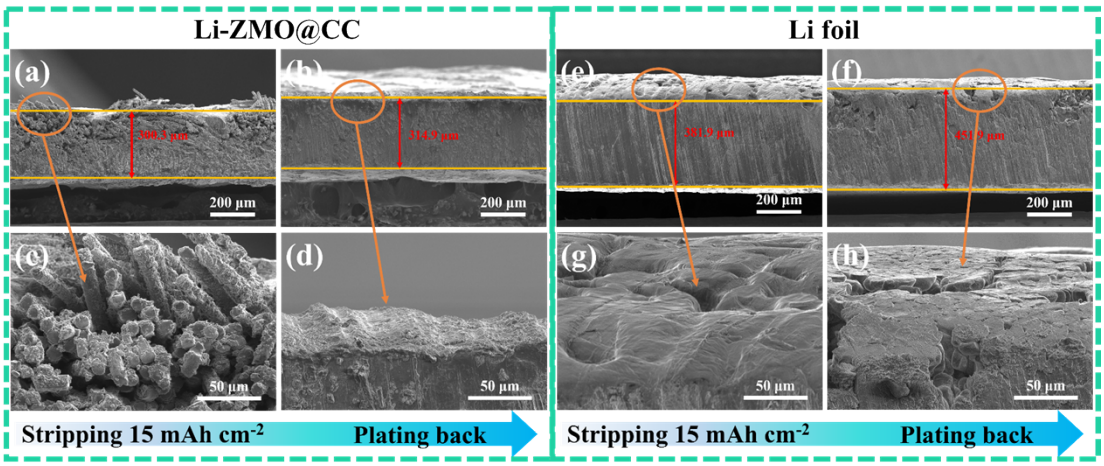

Fig. S10. Morphology evolution of Li-ZMO@CC and Li foil under different Li stripping/plating capacities. Cross-sectional SEM images of the Li-ZMO@CC after (a, c) stripping 15 mAh cm^{-2} Li and then (b, d) plating back 15 mAh cm^{-2} Li, Li foil after (e, g) stripping 15 mAh cm^{-2} Li and then (f, h) plating back 15 mAh cm^{-2} Li.

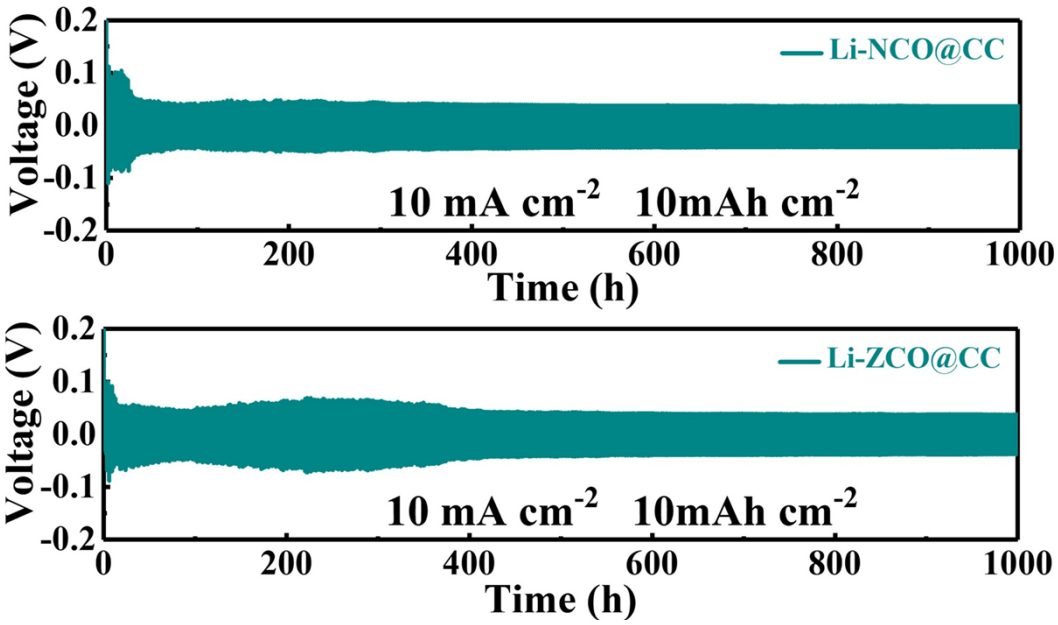

Fig. S11. Voltage profiles of Li-NCO@CC, Li-ZCO@CC anodes at 10 mAcm^{-2}/10 mAh cm^{-2}.

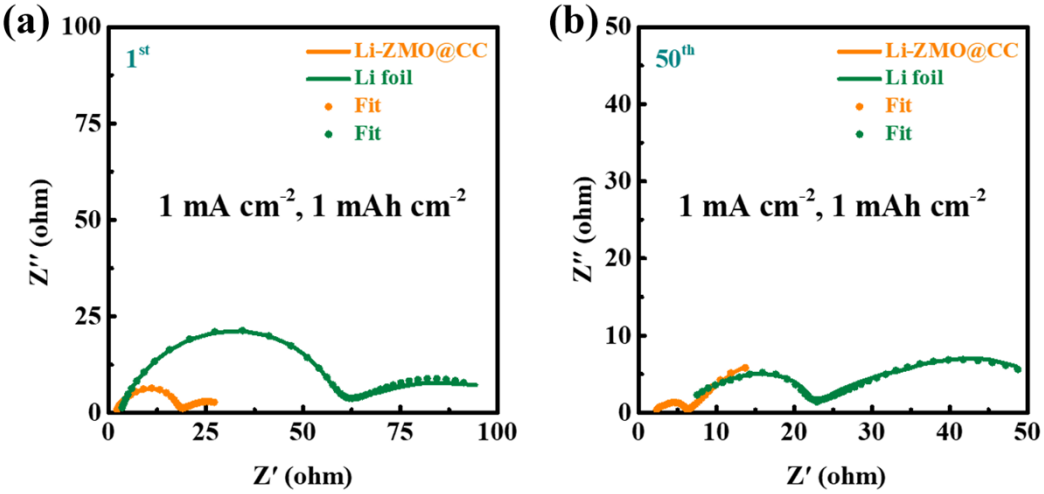

Fig. S12. Electrochemical impedance spectroscope (EIS) of composite Li anodes. EIS spectrum of Li-ZMO@CC and Li foil anodes after different cycles (b-c) at 1 mA cm^{-2}/1 mAh cm^{-2}.

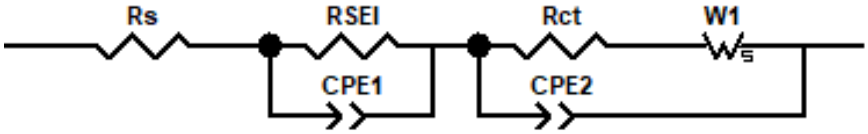

Fig. S13. The equivalent circuit of EIS.

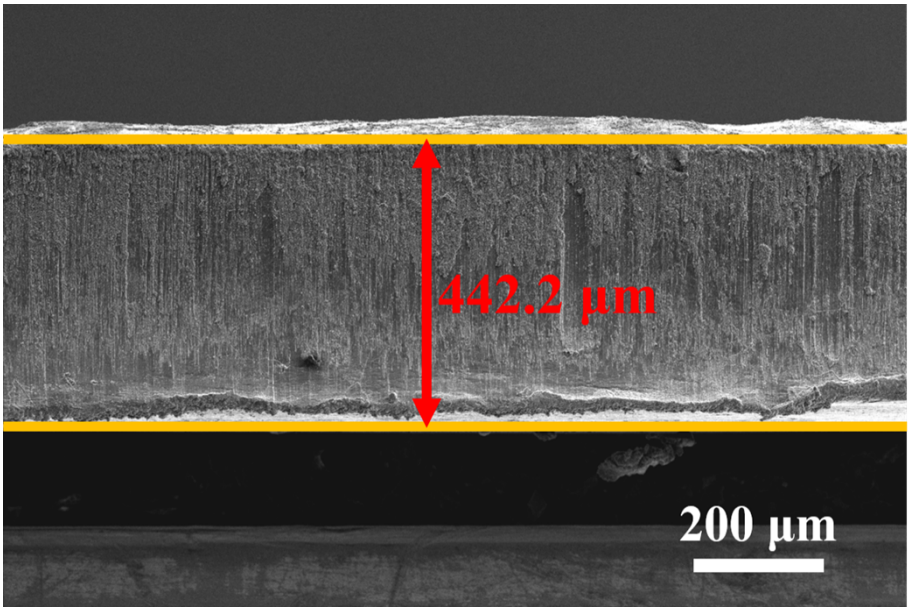

Fig. S14. The cross-sectional SEM image of Li foil at initial stage.

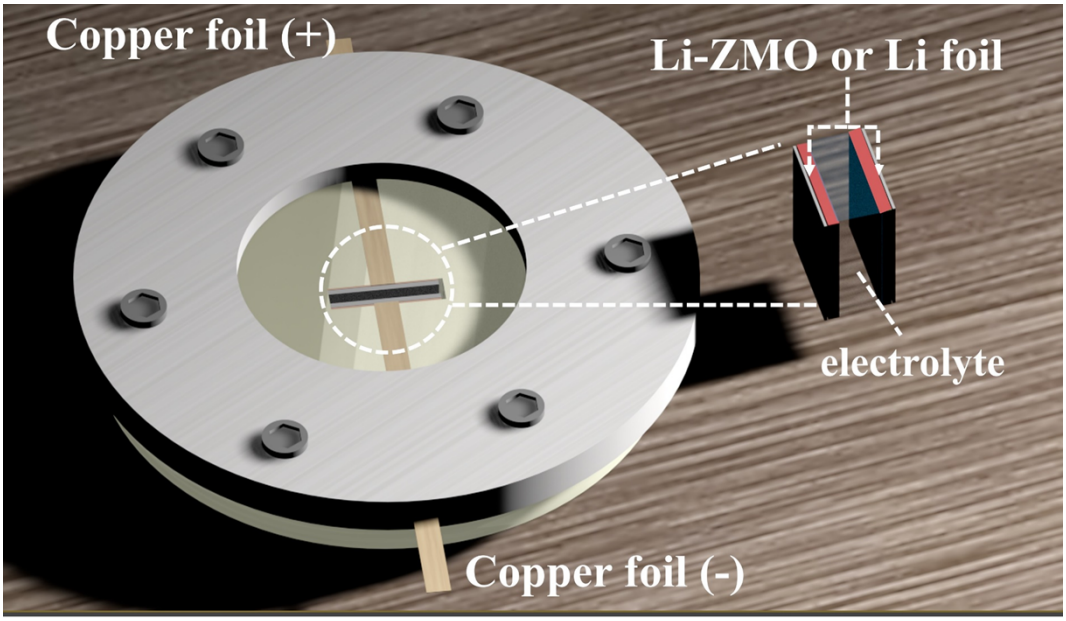

Fig. S15. The schematic diagram of electrochemical pool.

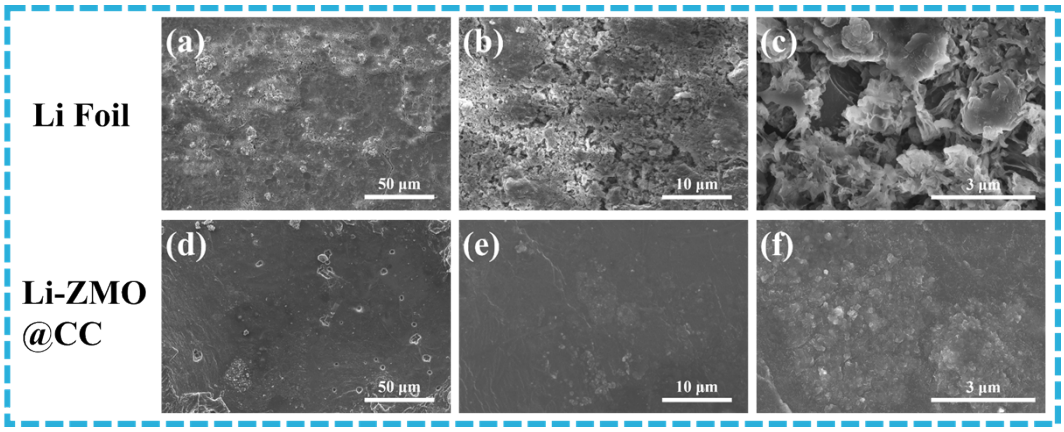

Fig. S16. Morphology evolution of full cells. The top-view SEM images of (a-c) Li|LFP and (d-f) Li-ZMO@CC|LFP anodes after 50th cycles at 2 C.

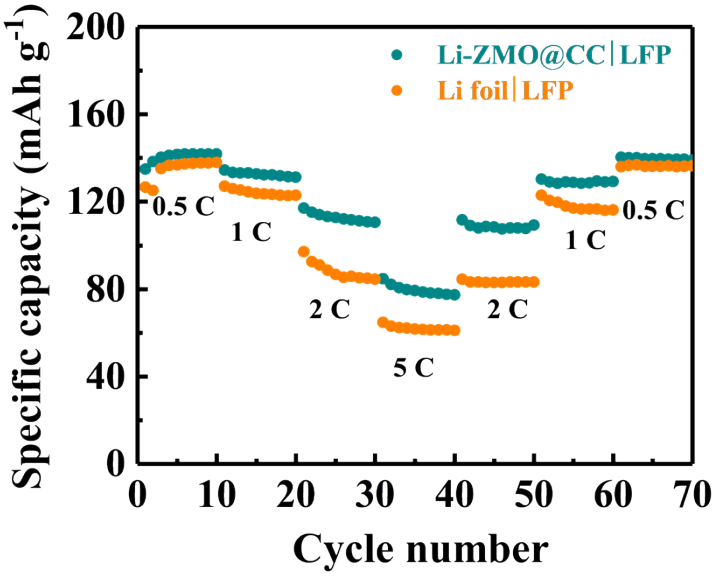

Fig. S17. Rate performance of Li-ZMO@CC|LFP and Li|LFP cells in the rate ranges from 0.5 to 5 C.

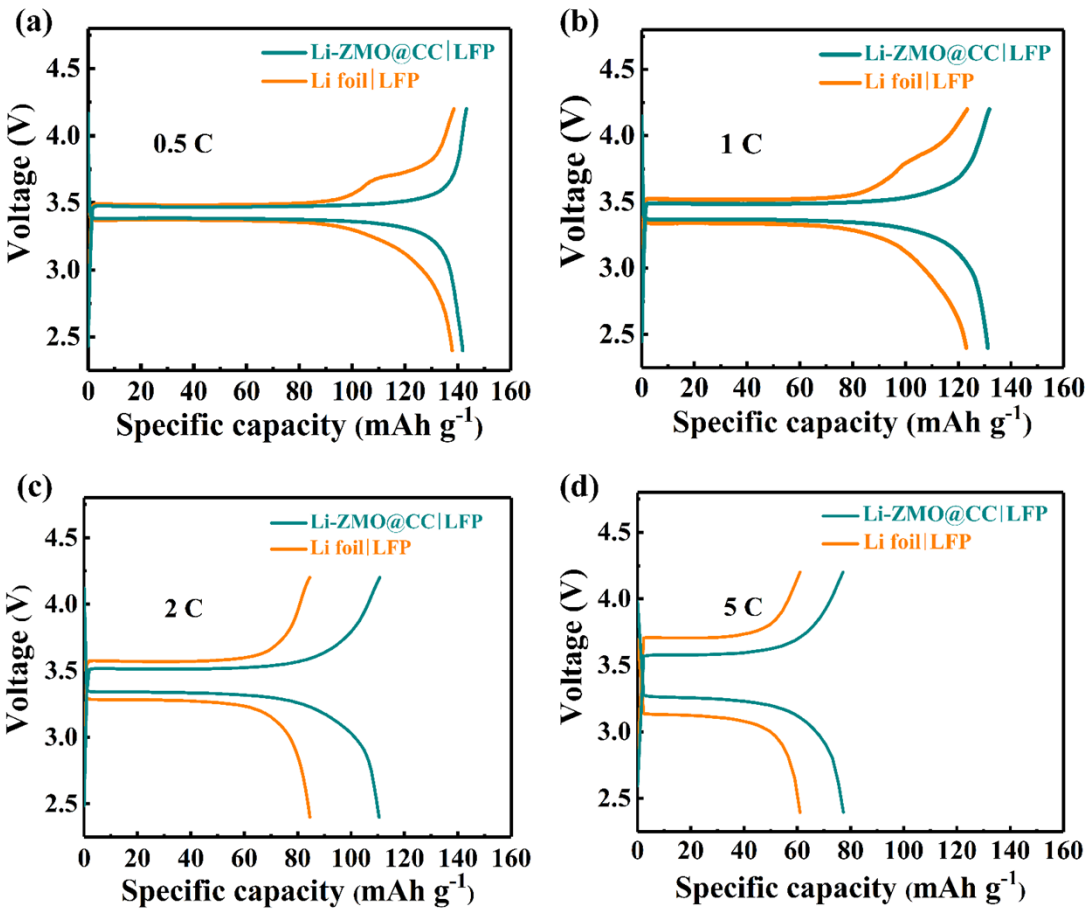

Fig. S18. Voltage hysteresis of full cells. Voltage profiles of Li-ZMO@CC|LFP and Li|LFP cells cycled at (a) 0.5, (b) 1, (c) 2, and (d) 5 C.

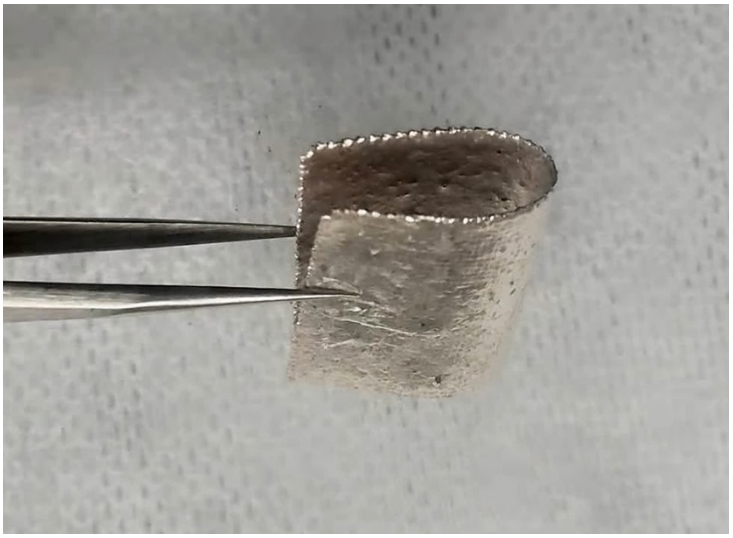

Fig. S19. The digital images in Li-ZMO@CC electrode under bending state.

Supplementary Table

Table S1. The calculated Gibbs free energy change of the reactions between bimetallic/ monometallic oxides and molten Li.

Materials	Gibbs Free Energy Change (300 °C)
$ZnMn_2O_4$ (ZMO)	-66.22 KJ/mol
$ZnCo_2O_4$ (ZMO)	-81.2 KJ/mol
$NiCo_2O_4$ (NCO)	-99.9 KJ/mol
ZnO	-111.35 KJ/mol
Mn_2O	-75.84 KJ/mol

Table S2. The cycle performances comparison of Li-ZMO@CC anode with previously reported Li metal anodes under various current densities and capacities.

Electrode	Current density ($mA\ cm^{-2}$)	Areal capacity ($mAh\ cm^{-2}$)	Time (h)
This work	5	10	1200
	5	20	500
	10	10	1900
Li-NCH@CF[1]	3	3	500
rGO-Ag-S-CNT[2]	2	1	500
Ag@CMFs-Li[3]	10	2	300
CNT/NiO@Li[4]	3	3	900
ZnO-MCNCF[5]	10	10	1400
Cu@MC@Li[6]	3	1	150
Li-Mn/G foam[7]	2	1	300
Cu@AuGA-Li[8]	4	4	1200

Table S3. The equivalent circuit fitting results of EIS measurements for Li foil and Li-ZMO@CC anodes.

Anode	Li foil			Li-ZMO@CC		
	$R_s(\Omega)$	$R_{SEI}(\Omega)$	$R_{ct}(\Omega)$	$R_s(\Omega)$	$R_{SEI}(\Omega)$	$R_{ct}(\Omega)$
1st	3.191	51.24	1.729	1.873	4.262	11.03
50th	5.743	8.479	6.019	2.076	1.816	2.206

References

[1] C. Chen, J. Guan, N.W. Li, Y. Lu, D. Luan, C.H. Zhang, G. Cheng, L. Yu, X.W. Lou, Lotus-Root-Like Carbon Fibers Embedded with Ni–Co Nanoparticles for Dendrite-Free Lithium Metal Anodes, Advanced Materials, (2021) 2100608.

[2] X.L. Li, S. Huang, D. Yan, J. Zhang, D. Fang, Y. Von Lim, Y. Wang, T.C. Li, L. Yifan, L. Guo, Tuning lithiophilicity and stability of 3D conductive scaffold via covalent Ag-S bond for high-performance lithium metal anode, Energy & Environmental Materials.

[3] Y. Fang, S.L. Zhang, Z.-P. Wu, D. Luan, X.W.D. Lou, A highly stable lithium metal anode enabled by Ag nanoparticle–embedded nitrogen-doped carbon macroporous fibers, Science Advances, 7 (2021) eabg3626.

[4] Y. Mei, J. Zhou, Y. Hao, X. Hu, J. Lin, Y. Huang, L. Li, C. Feng, F. Wu, R. Chen, High-Lithiophilicity Host with Micro/Nanostructured Active Sites based on Wenzel Wetting Model for Dendrite-Free Lithium Metal Anodes, Advanced Functional Materials, (2021) 2106676.

[5] R. Zhang, Y. Li, L. Qiao, D. Li, J. Deng, J. Zhou, L. Xie, Y. Hou, T. Wang, W. Tian, Atomic layer deposition assisted superassembly of ultrathin ZnO layer decorated hierarchical Cu foam for stable lithium metal anode, Energy Storage Materials, 37 (2021) 123-134.

[6] J. Qian, S. Wang, Y. Li, M. Zhang, F. Wang, Y. Zhao, Q. Sun, L. Li, F. Wu, R. Chen, Lithium Induced Nano-Sized Copper with Exposed Lithiophilic Surfaces to Achieve Dense Lithium Deposition for Lithium Metal Anode, Advanced Functional Materials, 31 (2021) 2006950.

[7] B. Yu, T. Tao, S. Mateti, S. Lu, Y. Chen, Nanoflake arrays of lithiophilic metal oxides for the ultra-stable anodes of lithium-metal batteries, Advanced Functional Materials, 28 (2018) 1803023.

[8] T. Yang, L. Li, F. Wu, R. Chen, A Soft Lithiophilic Graphene Aerogel for Stable Lithium Metal Anode, Advanced Functional Materials, 30 (2020) 2002013.